Not to appear in Nonlearned J., 45.

A 4–6 GHz Spectral Scan and 8–10 GHz Observations of the Dark Cloud TMC-1

S. V. Kalenskii

Astro Space Center, Profsoyuznaya 84/32 117997 Moscow, Russia

kalensky@asc.rssi.ru

V. I. Slysh

Arecibo Observatory, Arecibo, PR, USA

Astro Space Center, Profsoyuznaya 84/32 117997 Moscow, Russia

vslysh@asc.rssi.ru

P. F. Goldsmith

Department of Astronomy, Cornell University, and National Astronomy and Ionosphere Center, Ithaca, NY 14853, USA

goldsmit@astrosun.astro.cornell.edu

and

L. E. B. Johansson

Onsala Space Observatory. SE-439 92 Onsala, Sweden

leb@oso.chalmers.se

ABSTRACT

The results of the lowest frequency spectral survey carried out toward a molecular cloud and sensitive observations at selected frequencies are presented. The entire Arecibo C-band (4–6 GHz) was observed towards the cyanopolyyne peak of TMC-1 with an rms sensitivity of about 17–18 mK (about 2–2.5 mJy). In addition, a number of selected frequency ranges within the C-band and X-band (8–10 GHz) were observed with longer integration times and rms sensitivities 7–8

mK ($\approx$ 2 mJy) or higher. In the spectral scan itself, already–known H_2CO and HC_5N lines were detected. However, in more sensitive observations at selected frequencies, lines of C_2S, C_3S, C_4H, C_4H_2, HC_3N and its ^{13}C substituted isotopic species, HC_5N, HC_7N, and HC_9N were found, about half of them detected for the first time. The rotational temperatures of the detected molecules fall in the range 4–9 K. Cyanopolyyne column densities vary from 5.6×10^{13} cm^{-2} for HC_5N to 2.7×10^{12} cm^{-2} for HC_9N. Our results show that for molecular observations at low frequencies (4–10 GHz) to be useful for studying dark clouds, the sensitivity must be of the order of 5–10 mK or better. To date, observations at around 10 GHz have been more productive than those at lower frequencies.

Subject headings: ISM: individual (TMC-1)—ISM: molecules—ISM: clouds—radio lines: ISM

1. Introduction

Most known interstellar molecules have been detected in the millimeter wavelength range. This is clearly related to the fact that, in general, the simplest and hence the lightest molecules are the most abundant cosmic molecular species. Their strongest rotational lines at the temperatures characteristic of the molecular interstellar medium arise at mm and submm wavelengths. Heavier molecules, often with large permanent dipole moments, have detectable rotational lines at lower frequencies in the microwave range. Transitions between low energy levels are more favorable in terms of line intensities, especially in regions of low or modest density and low temperature. The latter include, in particular, the inner parts of dark clouds, which are among the coldest regions of the interstellar medium, because they have no internal energy sources and are shielded from external sources of radiation by their own gas and dust.

Another reason why observations at low frequencies are needed is the fact that the line intensities of molecules having fractional abundance below approximately 10^{-11} relative to H_2 fall below the confusion level in the millimeter wavelength range. In such cases, sensitive observations at low frequencies, which are less "contaminated" by the emission of simple molecules, may help. In addition, hyperfine splitting is often negligible at high frequencies, but detectable at low frequencies (e.g. for species HC_5N, HC_7N, etc.). Hyperfine splitting may be used to determine line opacities and thus to obtain more accurate molecular column densities and abundances.

Spectral scans, covering wide ranges of frequencies, are powerful tools for molecular

searches. Typically many lines of the same molecule fall within the observed spectral window, making it possible to more reliably identify observed spectral features. A number of spectral scans of molecular clouds have so far been carried out in atmospheric windows between 17 GHz and 700 GHz. A selection of the frequency ranges covered and references are 17.6–22 GHz (Bell et al. 1993); 72–144 GHz (Cummins et al. 1986; Johansson et al. 1984; Turner 1991); 330–360 GHz (Jewell et al. 1989); 455–507 GHz, (White et al. 2003); 607–725 GHz, (Schilke et al. 2001); 780–900 GHz, (Comito et al. 2002). Recently, Kaifu et al. (2004) carried out a spectral scan of the dark cloud TMC-1 in the frequency range between 8.8 and 50 GHz. However, no spectral scan has been performed at frequencies below 8.8 GHz. Therefore we undertook a spectral survey of TMC-1 at 4–6 GHz. This is the lowest frequency spectral survey carried out toward a molecular cloud[1].

TMC-1 has a shape of a ridge elongated in the northwest-southeast direction. The structure and chemical composition of TMC-1 have been studied by Hirahara et al. (1992), Pratap et al. (1997), Turner et al. (2000), and Dickens et al. (2001). The temperature of this object is about 10 K, which is typical for dark clouds; the H_2 density estimates towards the "cyanopolyyne peak" (see below) vary between 4×10^3 cm^{-3} (Turner et al. 2000) and 2×10^4 cm^{-3} (Pratap et al. 1997). The study by Peng et al. (1998) revealed 45 clumps which are grouped into 3 cylindrical features oriented along the ridge. The LSR velocities of these features are approximately 5.7, 5.9, and 6.1 km s^{-1}. TMC-1 has proven to be an excellent object for the study of chemistry in dark clouds under quiescent conditions. It shows a carbon–rich chemistry with chemical gradients across the densest part of the ridge extending over 0.2 pc x 0.6 pc. The most prominent chemical feature of TMC-1 is the high abundance of various carbon–chain molecules, such as cyanopolyynes $HC_{2n+1}N$ and radicals C_nH. The peak position of the line intensities of cyanopolyynes (the cyanopolyyne peak) was found to be located $\approx 7'$ southeast from another prominent position in TMC-1, the peak of the ammonia line emission. The heaviest known interstellar molecule, $HC_{11}N$, as well as a number of other heavy molecules have been found exactly towards the cyanopolyyne peak, making it an especially interesting object for observations at low frequencies.

2. Observations

The observations were performed with the 305-m radio telescope of the Arecibo Observatory. The entire Arecibo C-band (4–6 GHz) was observed towards the cyanopolyyne peak

[1]A similar spectral scan of IRC+10216 has been performed using the Arecibo telescope by Araya et al. (2003).

position ($\alpha_{1950} = 04^h38^m38^s$, $\delta_{1950} = 25°35'45''$). The C-band observations were performed in total power mode which is effective as a result of the excellent system stability, and which maximizes the signal to noise ratio. Two senses of linear polarization were independently observed and the two outputs averaged together. The four correlator boards of the spectrometer were offset in frequency by 5.25 MHz, and each was set to a bandwidth of 6.25 MHz, thus yielding an instantaneous continuous frequency coverage of 21 MHz with a frequency resolution of 3 kHz (0.183 km s^{-1} at 5 GHz). Each frequency setup was observed for 5 minutes. The entire C-band was observed 3 times, with one observation shifted by 3 MHz, yielding an rms sensitivity of about 17–18 mK (about 2–2.3 mJy).

In addition, a number of selected frequency ranges within the C-band and X-band (8–10 GHz) were observed with longer integration times and rms sensitivities 7–8 mK or higher. The X-band observations were performed in two senses of circular polarization. The beam size was about $0.'9 \times 1.'0$ in C-band and about $0.'5 \times 0.'5$ in X-band. The gain was about 8 K/Jy in C-band and about 4 K/Jy in X-band. The frequency ranges were centered at the frequencies of different molecular transitions taken from the JPL catalog of line positions and intensities (http://spec.jpl.nasa.gov/ftp/pub/catalog/catform.html) and the Cologne database for molecular spectroscopy (http://www.ph1.uni-koeln.de/vorhersagen/), as well as from the catalog of known molecular lines by F. Lovas (http://physics.nist.gov/cgi-bin/micro/table5/start.pl).

Each scan of the total power observations consisted of 50 6–second ON SOURCE observations followed by two 10–second calibration scans. The first of these calibration scans was taken with a noise diode switched on, and the second with the noise diode off. The data were calibrated by dividing the ON SOURCE spectra by the calibration spectra; the latter were calculated as the difference of the two calibration signal scans. To optimize the accuracy of the calibration while minimizing the effect of noise in the calibration scans, the calibration scans were approximated by polynomials of order 20 to 29. Polynomoials of low order (up to 3) were applied to remove residual baselines from the calibrated spectra. Both the calibration and subsequent data reduction were performed with the CLASS software package.

Lines with resolved hyperfine structure (i.e., when the hyperfine components are presented as different entries in Table 1) were fitted using the standard CLASS method HFS. This method enables us to derive the optical depth of the strongest component from the relative intensities of the observed components assuming that the excitation temperatures, LSR velocities, and linewidths of individual components are the same.

3. Results and analysis

TMC-1 has a very narrow lines of less than 0.4 km s^{-1} width. In order to achieve high velocity resolution of 0.18 km s^{-1} with the available number of spectrometer channels the entire band of 4–6 GHz was divided into 381 spectra. A portion of one of the C–band spectrum is shown in Fig. 1[2]. As a result of the spectral scan itself, we detected only lines of H_2CO and HC_5N. However, in more sensitive observations at selected frequencies in C– and X–bands we detected lines of C_2S, C_3S, C_4H, C_4H_2, HC_3N and its ^{13}C substituted isotopic species, HC_5N, HC_7N, and HC_9N. The $J = 5 - 4$ line of HC_7N and all lines of HC_9N, C_4H_2, CCS, and C_3S are new, i.e., they were not included in the catalog of known interstellar lines by F. Lovas at the time of writing this paper. The list of the detected lines with their fitted Gaussian parameters is presented in Table 1.

Most of our results were analysed with rotational diagrams. To construct rotational diagrams, we derived a rotational level population from the total intensity of relevant hyperfine components.

For optically thin emission, the integrated line intensity, W (K cm s^{-1}), is related to the upper level column density N_u by the well-known relation:

$$\frac{N_u}{g_u} = \frac{3kW}{8\pi^3\nu_0 S\mu^2} \frac{J(\nu, T_{ex})}{J(\nu, T_{ex}) - J(\nu, T_{bg})} , \quad (1)$$

where S is the line strength, μ is the permanent electric dipole moment, and $J(\nu, T) = h\nu/k \cdot [e^{(h\nu/kT)} - 1]^{-1}$. At low frequencies, where $h\nu \ll kT$, $J(T, \nu)$ is approximately equal to T. T_{ex} and T_{bg} are the excitation temperature and the background brightness temperature, respectively. If $J(\nu, T_{ex}) \gg J(\nu, T_{bg})$, the term $[J(\nu, T_{ex})]/[J(\nu, T_{ex}) - J(\nu, T_{bg})]$ approaches unity. In this case, assuming LTE and applying Boltzmann's equation, one can obtain from Eq. (1):

$$\ln \frac{3kW}{8\pi^3\nu_0 S\mu^2} = \ln \frac{N}{Q_{rot}} - \frac{E_u}{kT_{rot}} , \quad (2)$$

where E_u is the energy of the upper level of the transition, Q_{rot} is the partition function, and T_{rot} is the excitation temperature characterizing the rotational transitions of interest. Using Eq. (2), one can obtain the total molecular column density N and rotational temperature T_{rot} from observations of several lines of the same molecule. However, in the case of HC_5N and some other molecules the rotational temperature is fairly low; hence, the assump-

[2]All spectra are available at http://tanatos.asc.rssi.ru/ kalensky/scan.html

tion $J(T_{ex},\nu) \gg J(T_{bg},\nu)$ is not valid, and the term $[J(\nu,T_{ex})]/[J(\nu,T_{ex}) - J(\nu,T_{bg})]$ must be taken into account. Therefore we derived N and T_{rot} applying the following iterative approach:

1. Determination of "initial guesses" of T_{rot} and N from Eq. (2)
2. Calculation of $[J(\nu,T_{rot})]/[J(\nu,T_{rot}) - J(\nu,T_{bg})]$ from the estimate of T_{rot}
3. Determination of the next estimate of T_{rot} and N using the calculated value of $[J(\nu,T_{rot})]/[J(\nu,T_{rot}) - J(\nu,T_{bg})]$

Steps 2 and 3 were repeated until convergence was achieved. The calculated rotational temperatures and column densities are given in Table 2

For C_4H and C_4H_2, no rotational diagrams were constructed. To estimate column densities of these species, we assumed that the energy level populations are thermalized at a temperature taken from the literature and presented in Table 2. First, the optical depths of the observed lines were determined from the relation $\tau = T_R/(J(T_{ex},\nu) - J(T_{bg},\nu))$, where T_R is the main beam brightness temperature. Then, using the prescription from the secton "INTENSITY UNITS AND CONVENTIONS" of the JPL catalog documentation (http://spec.jpl.nasa.gov/ftp/pub/catalog/doc/catdoc.pdf) absorption coefficients per molecule per km s^{-1}, σ_{ba}, were found. Column densities N were obtained using the relation $\tau = \sigma_{ba}\ N$. The same technique was applied to obtain the upper limits to the column density presented in Table 3.

3.1. HC_3N, $H^{13}CCCN$, $HC^{13}CCN$, and $HCC^{13}CN$.

The spectra of the $J = 1 - 0$ HC_3N emission are shown in Fig 2. One sees a complex line profile, already found in a number of other molecular lines, and explained in terms of the existence of small-scale structure in TMC-1 (Dickens et al. 2001; Peng et al. 1998). Following Peng et al. (1998), who distinguished three main kinematic components towards TMC-1, we approximated the hyperfine–split line by a sum of three kinematic components with their intensities, LSR velocities, and linewidths free. The LSR velocities of the components proved to be 5.69, 5.85, and 6.06 km s^{-1}, which are approximately coincident with the velocity components determined by Peng et al. and by Dickens et al. A very limited number of offset measurements were performed which showed that (1) the peak of the 5.69 km s^{-1} emission is located approximately 40 arcsec south; (2) the peak of the 5.85 km s^{-1} emission is located approximately 30 arcsec southeast; and (3) the peak of the 6.06 km s^{-1} emission is located

approximately 40 arcsec north of the nominal position. However, both the extent and the sampling of our "map" are insufficient to determine the spatial distribution of the HC_3N emission.

The optical depth of the main hyperfine component is fairly small (about 0.2 for the 5.69 and 5.85 km s^{-1} components); however, it is in agreement with optical depths about unity for the higher frequency transitions reported by, e.g., Sorochenko et al. (1986). Therefore, simple methods of analysis, such as rotation diagrams, are not adequate (the formal use of the basic rotation diagram method yields a rotational temperature of 2 K), and a statistical equilibrium (SE) analysis which allows for effects of finite optical depth should be used (see e.g. Goldsmith & Langer 1999).

In addition to the main species, we detected the $J = 1 - 0$ $HCC^{13}CN$ emission and marginally detected two other ^{13}C substituted isotopomers, $HC^{13}CCN$ and $H^{13}CCCN$. The weakness of the lines of the ^{13}C–subsituted species did not allow us to measure reliably the isotopic abundance ratios, but the results seem to be in a qualitative agreement with the previous results of Takano et al. (1998), obtained from the observations of the $J = 2 - 1$, $4 - 3$, and $5 - 4$ lines at higher frequencies, i.e., the $HCC^{13}CN$ emission is the strongest and the $HC^{13}CCN$ and $H^{13}CCCN$ emission is weaker by a factor of 1.3. The ratio of the $HC_3N/HCC^{13}CN$ line intensities, 54 ± 15 is also in agreement with the ratio of $HC_3N/HCC^{13}CN$ abundances of 55 found by Takano et al., indicating a small optical depth for the lines observed using Arecibo.

3.2. HC_5N.

We detected $J = 2 - 1$ emission of HC_5N (Fig. 3). The ratio between the intensities of different hyperfine components corresponds to LTE with small optical depth. Combining our line intensity with the intensities of different lines of HC_5N published by Snell et al. (1981), in a rotational diagram (Fig. 6) we derive a HC_5N rotational temperature of 4.3 K, in agreement with e.g., Bell et al. (1998), and a column density of 5.6×10^{13} cm^{-2}.

3.3. HC_7N.

The $J = 5 - 4$, $7 - 6$, and $8 - 7$ lines were observed and spectra are shown in Fig. 3. The rotation diagram (Fig. 6) was constructed assuming HC_7N source size of $6' \times 1.'3$ (Bell et al. 1998), and yields a rotational temperature of 7.7 K and a HC_7N column density of 1.2×10^{13} cm^{-2}.

3.4. HC_9N.

We detected the $J = 15 - 14$ and $16 - 15$ transitions of HC_9N, and marginally detected the $J = 9 - 8$, $10 - 9$, and $14 - 13$ lines. The $J = 7 - 6$ line was not found because of the weakness of the rotational transition and its hyperfine splitting (Fig. 4). Rotational diagrams were constructed assuming a source size equal to $6' \times 1.'3$ (Fig. 6, upper right) and $100'' \times 55''$, suggested by Bell et al. (1998) (Fig. 6, lower right). One can see that the best fit to our data is obtained for the former source size. Thus, we derived a rotational temperature equal to 8.4 K and a HC_9N column density equal to 2.7×10^{12} cm^{-2}.

Our results on cyanopolyyne rotational temperatures are in agreement with the previous results by Bell et al. (1998), who found that the rotational temperatures of the cyanopolyynes increase with the number of heavy atoms over the range HC_5N–HC_9N and explained this effect in terms of less efficient radiative decay in the longer cyanopolyyne chains.

3.5. Other detected molecules

An unexpected result is the weakness of the tentatively detected $N_J = 3_2 - 2_2$ line of CCS at 5402.6 MHz relative to the 1–0 line of C_3S at 5780.8 MHz (Fig. 5). The CCS abundance is higher by an order of magnitude (Fuente et al. 1990), and usually CCS lines are much stronger than C_3S lines at approximately the same frequencies (e.g., Dickens et al. (2001)). The CCS line is intrinsically weaker than the C_3S line ($S \cdot \mu^2 = 13.76$ for the C_3S line and only 6.71 for the CCS line). The relevant rotational diagram (Fig. 6) yields a rotational temperature of 5.7 K and a CCS column density of 3.4×10^{13} cm^{-2}, which is in good agreement with that derived by means of a LVG analysis by Fuente et al. (1990). We derived the C_3S column density from LVG calculations, assuming $T_{kin} = 10$ K and $n_{H_2} = 3 \times 10^4$ cm^{-3} (Pratap et al. 1997). Our value, 3×10^{12} cm^{-2}, is in good agreement with that derived by Fuente et al. Thus, the weakness of the $3_2 - 2_2$ line of CCS is a consequence of its intrinsic weakness, the high location of its energy levels (E/k equals 10.84 K for the $N_J = 3_2$ CCS level), and the fairly low rotational temperature of CCS.

We detected a strong $N = 1 - 0$, $J = 3/2 - 1/2$, $F = 2 - 1$ transition of C_4H (Fig. 2), already observed in TMC-1 by Bell et al. (1982, 1983). The Arecibo line is narrow as a result of the weakness of the 6.06 km s^{-1} component towards the observed position. Since this component is fairly strong in the $1 - 0$ line of HC_3N, our data suggest that there is a difference between the small scale (about $30''$) distributions of HC_3N and C_4H. Note that the same C_4H line, observed with a much larger $3'.4$ beam (see Fig. 2 in Bell et al. (1982)), is broader, having a width of about 0.4 km s^{-1}, which is typical of TMC–1.

We believe that the detection of the $1_{01} - 0_{00}$ para-C_4H_2 line is real, since the C_4H_2 column density (derived from the line intensity under the assumptions that the C_4H_2 rotational temperature is 4.2 K and the ortho-to-para ratio is 4.2 (Kawaguchi et al. 1991)) is equal to 4.6×10^{12} cm^{-2}, which is comparable to, but somewhat smaller than, the value of 7.5×10^{12} cm^{-2} derived by Kawaguchi et al.

The $1_{10} - 1_{11}$ H_2CO line, detected using Arecibo (Fig. 1; Table 1) is rather similar but not identical to that observed previously by e.g., Henkel et al. (1981) with a $2'.6$ beam. The relative intensities of hyperfine components yielded the optical depth of the main component to be 1.6 and the line excitation temperature to be 1.2 K. No $1_{10} - 1_{11}$ $H_2^{13}CO$ and $H_2C^{18}O$ lines were detected. We estimate the lower limits to the ratios of the 1_{10} level populations for $H_2CO/H_2^{13}CO$ and $H_2CO/H_2C^{18}O$ assuming equal excitation temperatures for the $1_{10} - 1_{11}$ transition of all isotopic species. The limits are 24 and 76, which are below the $^{12}C/^{13}C$ and $^{16}O/^{18}O$ abundance ratios by factors of approximately 3 and 6, respectively. Thus, the non–detection of the $1_{10} - 1_{11}$ $H_2^{13}CO$ and $H_2C^{18}O$ lines does not contradict to the known values of the $^{12}C/^{13}C$ and $^{16}O/^{18}O$ abundance ratios.

3.6. Undetected lines

Table 3 presents the upper limits to the antenna temperatures of observed but undetected lines together with the relevant column density limits. The column density limits were calculated from Eq.(1) under the assumption that the line populations are thermalized at 10 K. Most of the molecular species from Table 3 have already been found in TMC-1 at higher frequencies. Comparison of the published column densities with the upper limits in Table 3 shows that an increase in sensitivity by a factor of 2–5 could lead to the detection of a much larger number of molecular lines. Thus, molecular observations at low frequencies (4–10 GHz) may be useful for studying dark clouds if the sensitivity (at 3σ level) is about 5–10 mK or better.

We did not estimate $H_2^{13}CO$ and $H_2C^{18}O$ column densities because of well-known strong deviations from LTE of the level populations of these species. Note that some other molecules may remain undetected in dark clouds due to excitation particularities rather than low abundances. For instance, CH_2NH was not detected in TMC-1 and L134 by Dickens et al. (1997); they suggested that it may be an excitation effect, since the observed transitions have critical densities of about 10^6 cm^{-3}, which is well below the density of TMC-1. Our non–detection of the $1_{10} - 1_{11}$ CH_2NH emission line is probably a result of the $1_{10} - 1_{01}$ transition at 167.4 GHz ($E_{low} = 2.135$ cm^{-1}), which can radiatively depopulate the 1_{10} level at the moderate densities found in TMC-1.

4. Summary

The results of the lowest frequency spectral survey carried out toward a dark cloud, studying TMC-1 in the 4–6 GHz range using the Arecibo radio telescope, and those from sensitive observations at selected frequencies in C– and X–bands can be summarized as follows:

- A number of molecular lines were detected. The majority of the detected lines belong to the cyanopolyynes HC_3N, HC_5N, HC_7N, and HC_9N.
- The rotational temperatures of the detected molecules fall in the range 4–9 K. Cyanopolyyne column densities vary from 5.6×10^{13} cm^{-2} for HC_5N to 2.7×10^{12} cm^{-2} for HC_9N.
- Molecular observations at low frequencies (4–10 GHz) can be useful for studying dark clouds, but to be really effective, the sensitivity must be increased by a factor of 2 to 3. To date, observations at around 10 GHz have been more fruitful than those at lower frequencies.

The National Astronomy and Ionosphere Center is operated by Cornell University under a cooperative agreement with the National Science Foundation. We are grateful to the staff of the Arecibo Observatory, and especially Jeff Hagen, Mike Nolan, Phil Perillat, Chris Salter, and Arun Venkataraman for help during the observations and useful discussions. We thank the anonymous referee for important comments. SVK's visit to Arecibo was supported by the NAIC Director's Office. The work was partly supported by the Russian Foundation for Basic Research (grant no. 01-02-16902).

REFERENCES

Araya, E., Hofner, P., Goldsmith, P. F., Slysh, V. I., & Takano, S. 2003, ApJ, 596, 556

Bell, M. B., Sears, T. J., & Matthews, H. E., 1982, ApJ, 255, L75

Bell, M. B., Matthews, H. E., & Sears, T. J., 1983, ApJ, 127, 241

Bell, M. B., Avery, L. W., & Watson, J. K. G., 1993, ApJS, 86, 211

Bell, M. B., Watson, J. K. G., Feldman, P. A., & Travers, M. J., 1998, ApJ, 508, 286

Comito, C., Schilke, P., Lis, D. C., Motte, F., Phillips, T. G., & Mehringer, D. M., 2002, SFChem 2002: Chemistry as a Diagnostic of Star Formation, C. L. Curry & M. Fish, to be published by NRC Press, Ottava, Canada, 18

Cummins, S. E., Linke, R. A & Thaddeus, P., 1986, ApJS, 60, 819

Dickens, J. E., Langer, W. D., & Velusamy, T., 2001, ApJ, 558, 693

Dickens, J. E., Irvine, W. M., & DeVries, C. H., 1997, ApJ, 479, 307

Fuente, A., Cernicharo, J., Barcia, A., & Gomez-Gonzales, J., 1990, A&A, 231, 151

Goldsmith, P.F. & Langer, W.D. 1999, ApJ, 517, 209

Guelin, M., Friberg, P., & Mezaoui, A., 1982, A&A, 109, 23

Henkel, C., Wilson, T. L., & Pankonin, V., 1981, A&A, 99, 270

Hirahara, Y., Suzuki, H., Yamamoto, S., Kawaguchi, K., Kaifu, N., Ohishi, M., Takano, S., Ishikawa, S.-I., & Masuda, A., 1992, ApJ, 394, 539

Jewell, P. R., Hollis, J. M., Lovas, F. J., & Snyder, L. E., 1989, ApJS, 70, 833

Johansson, L. E. B., Andersson, C., Ellder, J., Friberg, P., Hjalmarson, Å., Hoglund, B., Irvine, W. M., Olofsson, H., & Rydbeck, G., 1984, A&A, 130, 227

Kaifu, N., Ohishi, M. Kawaguchi, K., Saito, S., Yamamoto, S., Miyaji, T., Miyazawa, K., Ishikawa, S., Noumaru, C., Harasawa, S., and Okuda, M. 2004, PASJ, 56, No.1, 69

Kawaguchi, K., Kaifu, N., Ohishi, M., Ishikawa, S.-I., Hirahara, Y., Yamamoto, S., Saito, S., Takano, S., Murakami, A., Vrtilek, J. M., Gottlieb, C. A., & Thaddeus, P., 1991, PASJ, 43, 607

Ohishi, M., & Kaifu, N., 1998, Faraday Discussion, 109, 205

Peng, R., Langer, W. D., Velusamy, T., Kuiper, T. B. H., & Levin, S., 1998, ApJ, 497, 842

Pratap, P., Dickens, J. E., Snell, R. L., Miralles, M. P., Bergin, E. A., Irvine, W. M., & Schloerb, F. P., 1997, ApJ, 486, 862

Schilke, P., Benford, D. J., Hunter, T. R., Lis, D. C., & Phillips, T. G., 2001, ApJS, 132, 281

Snell, R. L., Schloerb, F. P., Young, J. S., Hjalmarson, Å., & Friberg, P., 1981, ApJ, 244, 45

Sorochenko, R. L., Tolmachev, A. M., & Winnewisser, G., 1986, A&A, 155, 237

Turner, B.E. 1991, ApJS, 76, 617

Turner, B. E., Herbst, E., & Terzieva, R., 2000, ApJS, 126, 427

Takano, S., Masuda, A., Hirahara, Y., Suzuki, H., Ohishi, M., Ishikawa, S., Kaifu, N., Kasai, Y., Kawaguchi, K., & Wilson, T. L., 1998, A&A, 329, 1156

White, G. J., Araki, M., Greaves, J. S., Ohishi, M., & Higginbottom, N. S., 2003, A&A, 407, 589

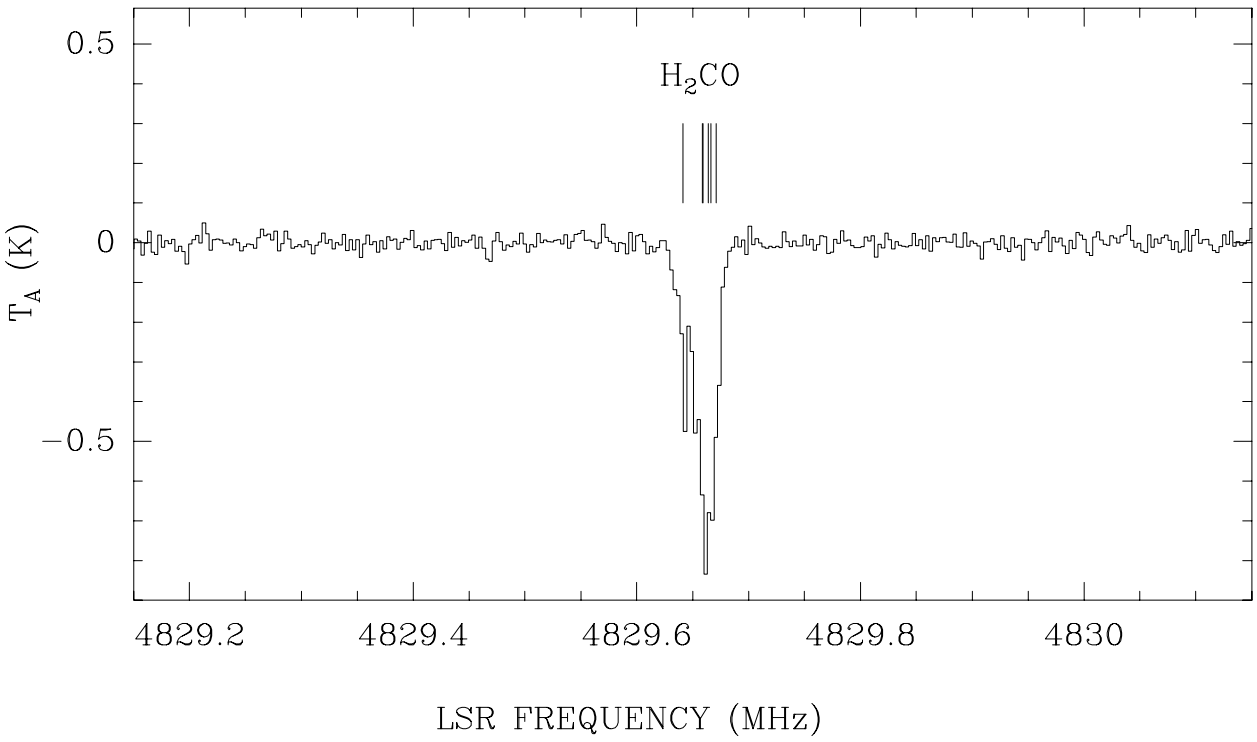

Fig. 1.— A 1 MHz portion of the C-band spectrum. The horizontal axis is the rest frequency in MHz and the vertical axis is the antenna temperature in Kelvins. The strong absorption line at the center is the $1_{10} - 1_{11}$ transition of H_2CO. The positions of the hyperfine components are shown by vertical bars.

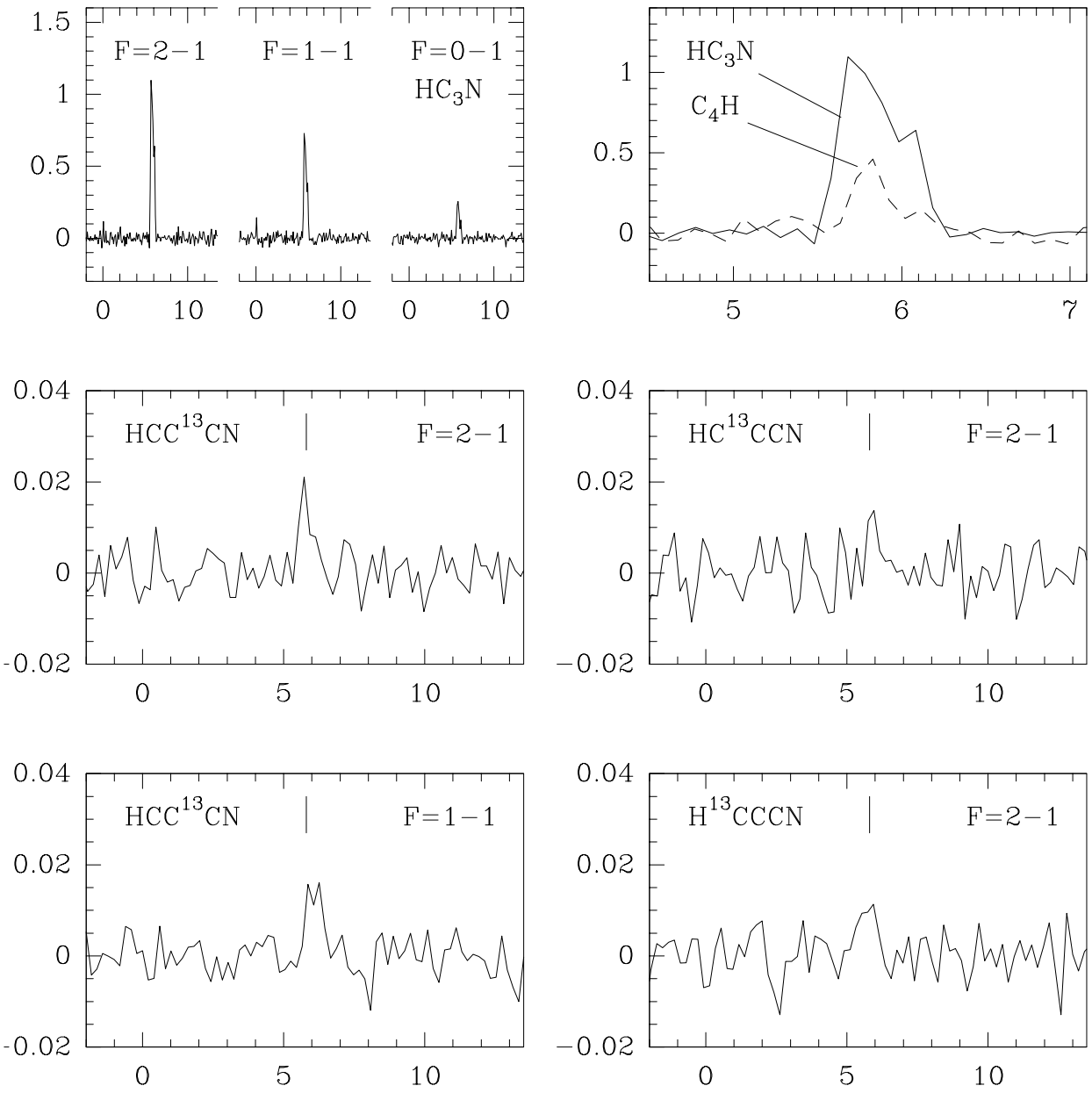

Fig. 2.— Spectra of the $J = 1 - 0$ transitions of HC_3N and ^{13}C substituted isotopic species. The horizontal axis is the LSR velocity in km s^{-1} and the vertical axis is the antenna temperature in Kelvins. The C_4H line at 9497.616 MHz is indicated by the dashed line in the plot at the upper right, together with the $F = 2 - 1$ line of HC_3N (solid line).

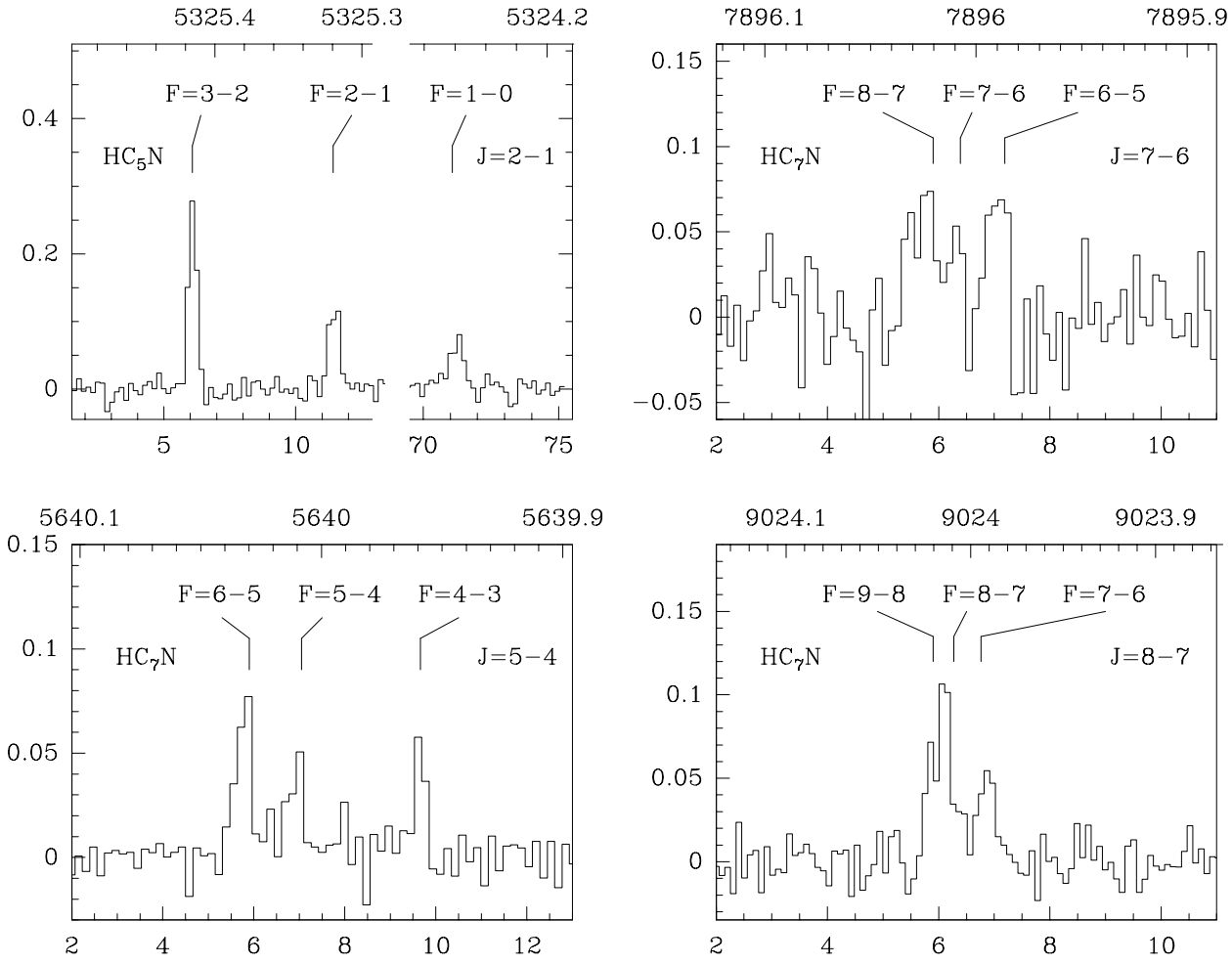

Fig. 3.— Spectra of cyanopolyynes HC_5N and HC_7N. The rotational transition is indicated in the upper right corner of each spectrum. The vertical lines indicate the positions of the hyperfine components. The upper horizontal axis plots the rest frequency in MHz and the lower horizontal axis is the LSR velocity of the strongest hyperfine component in km s^{-1}; the vertical axis is the same as in Fig. 2.

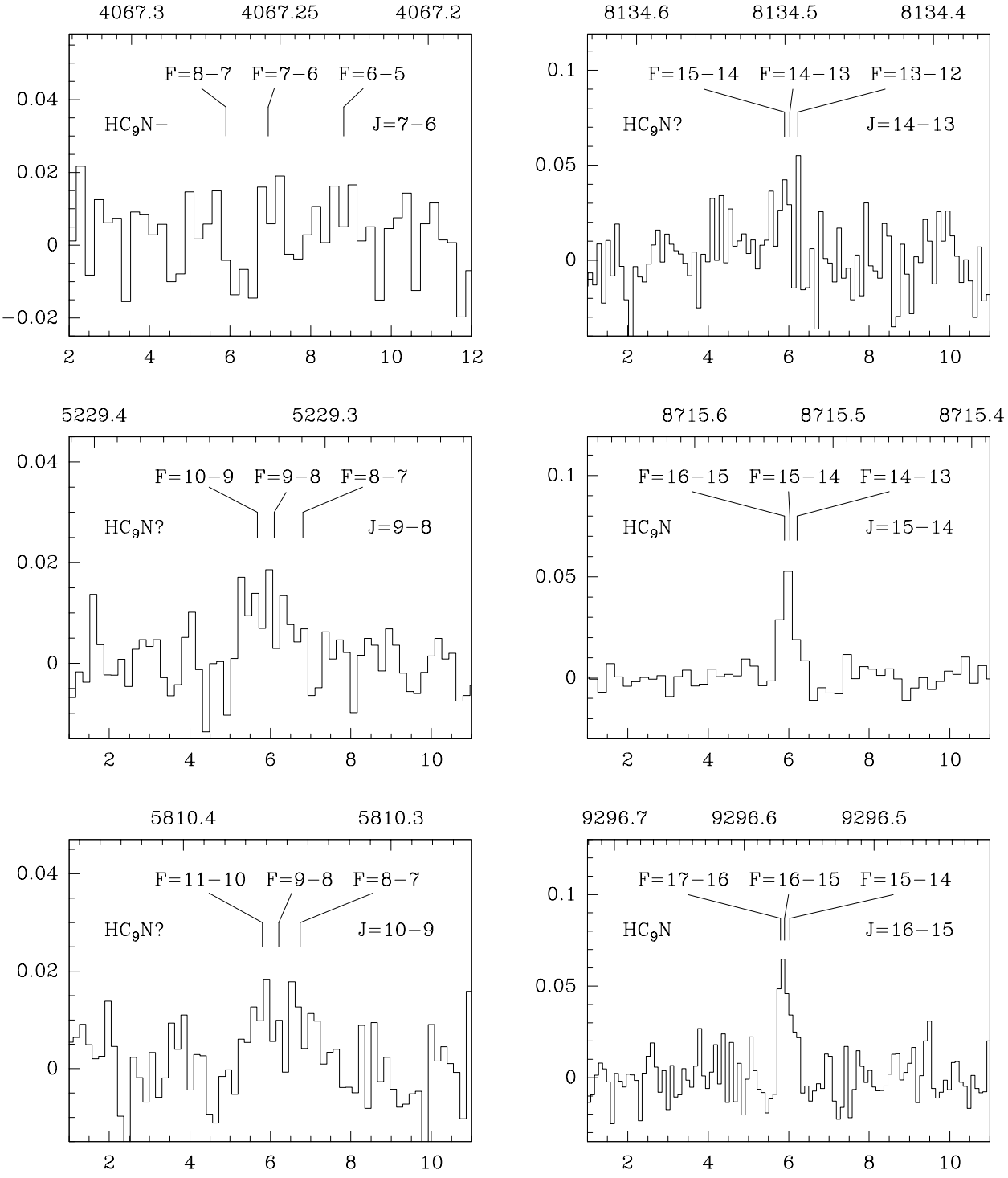

Fig. 4.— Various HC_9N lines. The rotational transition is indicated in the upper right corner of each spectrum. The vertical lines indicate the positions of the hyperfine components. A minus after the species name means that the line was not detected. A question mark after the species name denotes a marginal detection. The axes are the same as in Fig. 3.

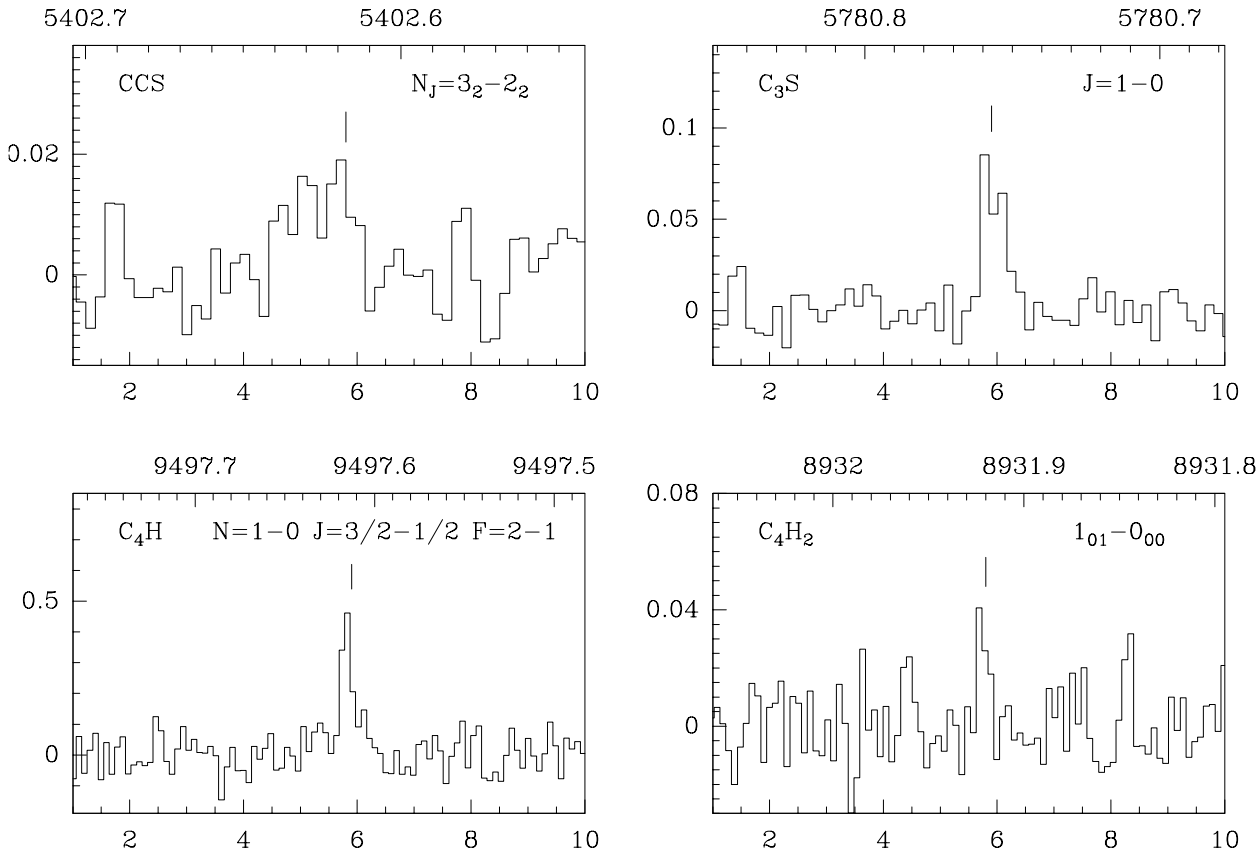

Fig. 5.— Spectra of CCS, C_3S, C_4H, and C_4H_2 transitions. The upper horizontal axis plots the rest frequency in MHz and the lower horizontal axis is the LSR velocity in km s^{-1}; the vertical axis is the same as in Fig. 2.

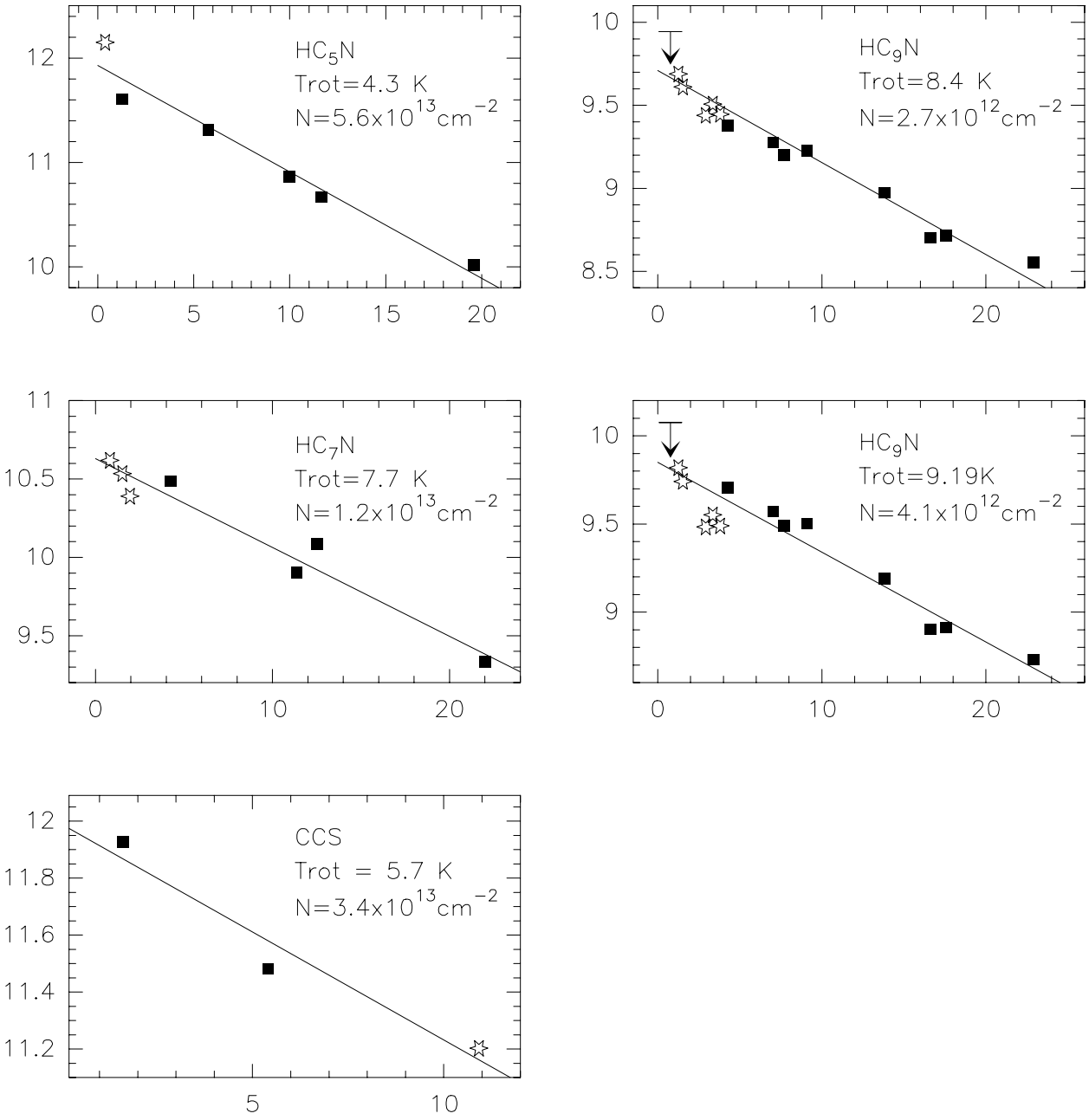

Fig. 6.— Rotation diagrams. The lines detected at Arecibo are denoted by stars, while filled squares represent the lines taken from the literature. Two different diagrams for HC_9N were constructed assuming different source sizes: $6' \times 1.'3$ (upper), and $1.7' \times 0.'9$ (lower). For each diagram, the horizontal axis is E_u/k and the vertical axis is $\log(3kW)/(8\pi^3\nu_0 S\mu^2)$ (see section 3).

Table 1. Gaussian fit parameters of the detected lines.

Molecule	Frequency (MHz)	Transition	$\int T_A^* dV$ K km s^{-1}	$V_{\rm LSR}$ km s^{-1}	ΔV km s^{-1}	T_A^* (K)
HC_3N	9097.0346	$J = 1 - 0$ $F = 1 - 1$	0.138(0.003)	5.689(0.002)	0.167(0.001)	0.684
			0.091(0.002)	5.851(0.003)	0.168(0.006)	0.512
			0.071(0.001)	6.061(0.003)	0.167(0.007)	0.400
HC_3N	9089.3321	$J = 1 - 0$ $F = 2 - 1$	0.180(0.012)	5.689(0.002)	0.167(0.001)	1.085
			0.136(0.007)	5.851(0.003)	0.168(0.006)	0.814
			0.115(0.003)	6.061(0.003)	0.167(0.007)	0.693
HC_3N	9100.2727	$J = 1 - 0$ $F = 0 - 1$	0.042(0.004)	5.689(0.002)	0.167(0.001)	0.240
			0.032(0.003)	5.851(0.003)	0.168(0.006)	0.180
			0.024(0.001)	6.061(0.003)	0.167(0.007)	0.137
$H^{13}CCCN$	8817.096	$J = 1 - 0$ $F = 2 - 1$	0.006(0.002)	5.66(0.14)	0.40(0.00)[1]	0.014
$HC^{13}CCN$	9059.736	$J = 1 - 0$ $F = 2 - 1$	0.007(0.002)	5.91(0.06)	0.40(0.00)[1]	0.015
$HCC^{13}CN$	9060.608	$J = 1 - 0$ $F = 2 - 1$	0.009(0.002)	5.72(0.04)	0.40(0.00)[1]	0.021
$HCC^{13}CN$	9059.318	$J = 1 - 0$ $F = 1 - 1$	0.008(0.002)	6.11(0.15)	0.40(0.00)[1]	0.018
HC_5N	5325.421	$J = 2 - 1$ $F = 3 - 2$	0.12(0.003)	5.91(0.01)	0.41(0.01)	0.28
HC_5N	5325.330	$J = 2 - 1$ $F = 2 - 1$	0.06(0.002)	5.91(0.01)	0.41(0.01)	0.15
HC_5N	5324.270	$J = 2 - 1$ $F = 1 - 0$	0.03(0.001)	5.91(0.01)	0.41(0.01)	0.07
HC_7N*	5640.0316	$J = 5 - 4$ $F = 6 - 5$	0.027(0.004)	6.00(0.02)	0.34(0.04)	0.075
HC_7N*	5640.0091	$J = 5 - 4$ $F = 5 - 4$	0.021(0.004)	6.00(0.02)	0.34(0.04)	0.061
HC_7N*	5639.9580	$J = 5 - 4$ $F = 4 - 3$	0.018(0.004)	6.00(0.02)	0.34(0.04)	0.049
HC_7N	7896.023	$J = 7 - 6$ $F = 8 - 7$	0.028(0.012)	5.92(0.04)	0.33(0.04)	0.080
HC_7N	7896.010	$J = 7 - 6$ $F = 7 - 6$	0.024(0.012)	5.92(0.04)	0.33(0.04)	0.069
HC_7N	7895.989	$J = 7 - 6$ $F = 6 - 5$	0.021(0.012)	5.92(0.04)	0.33(0.04)	0.060
HC_7N	9024.020	$J = 8 - 7$ $F = 9 - 8$	0.028(0.006)	5.94(0.02)	0.39(0.03)	0.069
HC_7N	9024.009	$J = 8 - 7$ $F = 8 - 7$	0.025(0.006)	5.94(0.02)	0.39(0.03)	0.061
HC_7N	9023.994	$J = 8 - 7$ $F = 7 - 6$	0.022(0.006)	5.94(0.02)	0.39(0.03)	0.053
HC_9N*	5229.3272	$J = 9 - 8$[2]	0.016(0.004)[3]	5.87(0.14)	1.11(0.23)	0.014
HC_9N*	5810.362	$J = 10 - 9$[2]	0.017(0.005)[3]	6.30(0.23)	1.51(0.39)	0.012
HC_9N*	8134.503	$J = 14 - 13$[2]	0.016(0.005)[3]	5.90(0.11)	0.57(0.21)	0.027
HC_9N*	8715.538	$J = 15 - 14$[2]	0.022(0.003)	5.96(0.02)	0.39(0.05)	0.053
HC_9N*	9296.5721	$J = 16 - 15$[2]	0.022(0.003)	5.91(0.03)	0.33(0.06)	0.061
CCS*	5402.6175	$N_J = 3_2 - 2_2$	0.009(0.003)[3]	5.70(0.07)	0.40(0.00)[1]	0.021
C_3S*	5780.759	$J = 1 - 0$	0.041(0.005)	5.91(0.01)	0.49(0.03)	0.077
C_4H	9497.616	$N = 1 - 0$ $J = 3/2 - 1/2$ $F = 2 - 1$	0.098(0.01)	5.77(0.01)	0.21(0.03)	0.447
C_4H_2*	8931.92	$1_{01} - 0_{00}$	0.009(0.003)[3]	5.72(0.01)	0.11(0.30)	0.079
H_2CO	4829.6594	$1_{10} - 1_{11}$ $F = 2 - 2$[4]	−0.533	5.84(0.01)	0.71(0.02)	−0.753

Table 1—Continued

Molecule	Frequency (MHz)	Transition	$\int T_A^* dV$ K km s^{-1}	$V_{\rm LSR}$ km s^{-1}	ΔV km s^{-1}	T_A^* (K)

[1]the line width is fixed

[2]the sum of the hyperfine components presented in Fig. 4

[3]marginal detection

[4]the strongest hyperfine component

Note. — The frequencies of the known lines are taken from the Lovas catalog of observed lines. The frequences of the newly detected lines (denoted by an asterisk after the species name) and all HC_7N lines are taken from the Cologne database for molecular spectroscopy. The numbers in parentheses denote the 1σ uncertainties of the corresponding values.

Table 2. Rotational temperatures and column densities for detected molecular species.

Molecule	$T_{\rm rot}$ (K)	Column density ($\rm cm^{-2}$)
HC_5N	4.3 ± 0.4	$(5.6 \pm 1.4) \times 10^{13}$
HC_7N	7.7 ± 0.7	$(1.2 \pm 0.2) \times 10^{13}$
HC_9N	8.4 ± 0.4	$(2.7 \pm 0.2) \times 10^{12}$
CCS	5.7 ± 1.0	$(3.4 \pm 0.8) \times 10^{13}$
C_4H	5.6[1]	1.1×10^{15}
C_4H_2	4.2[2]	4.2×10^{12}

[1]from Ohishi & Kaifu (1998).

[2]from Kawaguchi et al. (1991).

Note. — Errors are given at 1σ level. For cyanopolyynes and CCS the parameters were obtained by using rotation diagrams. For C_4H and C_4H_2, the column densities were calculated using rotation temperatures taken from the literature.

Table 3. Upper limits to the antenna temperatures for undetected lines and relevant molecular column density limits.

Molecule	Frequency (MHz)	Transition	$\|T_A^*\|$ upper limit (K)	Column density[1] upper limit (cm^{-2})	Reference for frequency[2]
HC_9N[3]	4067.2695[4]	$J = 7 - 6$	0.026		Col
$HC_{11}N$	5071.8851	$J = 15 - 14$	0.027	2.53×10^{12}	JPL
$HC_{11}N$	5410.0103	$J = 16 - 15$	0.012	1.01×10^{12}	JPL
$HC_{11}N$	8115.007	$J = 24 - 23$	0.033	2.41×10^{12}	JPL
$HC_{11}N$	8791.257	$J = 26 - 25$	0.042	3.12×10^{12}	JPL
$HC_{11}N$	9129.376	$J = 27 - 26$	0.018	1.29×10^{12}	JPL
$HC_{13}N$	5348.622	$J = 25 - 24$	0.012	1.33×10^{12}	Col
$HC_{13}N$	5562.566	$J = 26 - 25$	0.013	1.26×10^{12}	Col
C_4D	8868.9005	$N = 1 - 0$	0.033	2.25×10^{14}	Col
		$J = 1/2 - 1/2$			
C_5O	5467.388	$J = 2 - 1$	0.030	5.00×10^{12}	JPL
C_4S	5912.1755	$N_J = 3_2 - 2_1$	0.027	1.11×10^{13}	Col
C_4S	8868.7075	$N_J = 4_3 - 3_2$	0.033	1.04×10^{13}	Col
C_5S	5536.222	$J = 3 - 2$	0.029	4.43×10^{12}	JPL
C_5S	9227.028	$J = 5 - 4$	0.036	3.81×10^{12}	JPL
C_5N	5607.1377[4]	$N = 2 - 1$	0.030	2.56×10^{13}	Col
		$J = 5/2 - 3/2$			
C_6H	4201[5]	$^2\Pi_{1/2}$ $J = 3/2 - 1/2$	0.026	1.86×10^{13}	JPL
CH_3C_4H	4071.4935	$J_K = 1_0 - 0_0$	0.030	1.36×10^{14}	Col
CH_2NH	5289.813[4]	$1_{10} - 1_{11}$	0.030	3.54×10^{13}	Lov
HCOOH	4916.312	$2_{11} - 2_{12}$	0.039	9.63×10^{13}	Lov
CH_2CO	5660.9476	$5_{14} - 5_{15}$	0.024	3.68×10^{14}	JPL
$H_2C^{18}O$	4388.8011[4]	$1_{10} - 1_{11}$	0.021		Lov
$H_2^{13}CO$	4593.0865[4]	$1_{10} - 1_{11}$	0.072		Lov

[1]assuming a rotational temperature equal to 10 K

[2]JPL indicates the JPL catalog, Col the Cologne database, and Lov the Lovas line list

[3]HC_9N column density is presented in Table 2.

[4]blended hyperfine structure

[5]a line multiplet

Note. — The limits are given at 3σ level.